THE JOURNAL OF PHYSICAL CHEMISTRY B

Article

pubs.acs.org/JPCB

Aβ41 Aggregates More Like Aβ40 than Like Aβ42: In Silico and in Vitro Study

Hoang Linh Nguyen,[†,‡] Tran Thi Minh Thu,[†,‡] Phan Minh Truong,[†] Pham Dang Lan,[†] Viet Hoang Man,[§] Phuong H. Nguyen,[∥] Ly Anh Tu,[‡] Yi-Cheng Chen,[*,⊥] and Mai Suan Li[*,§]

[†]Institute for Computational Science and Technology, SBI Building, Quang Trung Software City, Tan Chanh Hiep Ward, District 12, Ho Chi Minh City, Vietnam

[‡]Department of Applied Physics, Faculty of Applied Science, Ho Chi Minh City University of Technology - VNU HCM, 268 Ly Thuong Kiet Street, District 10, Ho Chi Minh City, Vietnam

[§]Institute of Physics, Polish Academy of Sciences, Al. Lotnikow 32/46, 02-668 Warsaw, Poland

[∥]Laboratoire de Biochimie Theorique, UPR 9080 CNRS, IBPC, Universite Paris 7, 13 rue Pierre et Marie Curie, 75005 Paris, France

[⊥]Department of Medicine, MacKay Medical College, New Taipei City 252, Taiwan

ABSTRACT: Formation of intracellular plaques and small oligomeric species of amyloid β (Aβ) peptides inside neurons is a hallmark of Alzheimer's disease. The most abundant Aβ species in the brain are Aβ1-40 and Aβ1-42, which are composed, respectively, of 40 and 42 residues. Aβ1-42 differs from Aβ1-40 only in two residues, Ile41 and Ala42, yet it shows remarkably faster aggregation and greater neurotoxicity than Aβ1-40. Thus, it is crucial to understand the relative contributions of Ile41 and Ala42 to these distinct behaviors. To achieve this, secondary structures of the Aβ1-41 monomer, which contribute to aggregation propensity, were studied by all-atom molecular dynamics simulation in an implicit solvent and compared to those of Aβ1-40 and Aβ1-42. We find that the secondary structure populations of Aβ1-41 are much closer to those of Aβ1-40 than to those of Aβ1-42, suggesting that Aβ1-41 and Aβ1-40 are likely to have similar aggregation properties. This prediction was confirmed through a thioflavin-T aggregation assay. Thus, our finding indicates that the hydrophobic residue at position 42 is the major contributor to the increased fibril formation rates and consequently neurotoxicity of Aβ peptides.

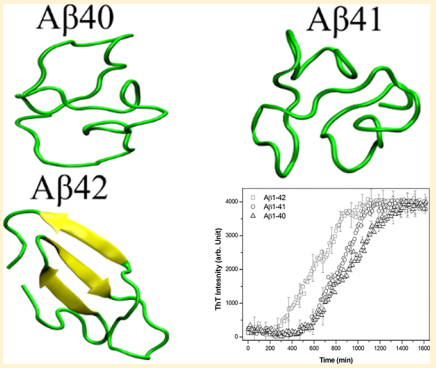

1. INTRODUCTION

Hallmarks of Alzheimer's disease (AD) are fibrillar plaques of amyloid β (Aβ) peptides formed around neurons in the brain.[1] Aβ peptides, which are proteolytic products of amyloid precursor protein (APP) on cleavage by β- and γ-secretases, have various lengths or numbers of amino acids. Together with Aβ1-40 and Aβ1-42, which are the most abundant, truncated Aβ1−26, Aβ1-30, Aβ1-39,[2] Aβ4-42, and Aβ5-42[3] are also found inside amyloid plaques. Variants longer than Aβ1-42, such as Aβ1-43, Aβ1-45, Aβ1-48, Aβ1-49, and Aβ1-50, were identified in cell lines,[4,5] transgenic mice,[6] and eventually in the human brain.[7−9] They polymerize even faster than Aβ1-42, being more hydrophobic and consequently more neurotoxic. Although the level of Aβ1-43 in the human brain, for instance, is low compared to that of Aβ1-40 and Aβ1-42, it has been suggested that Aβ1-43 could form oligomers and amyloid plaques and thereby be instrumental to AD pathogenesis.[9,10]

Because Aβ1-40 and Aβ1-42 peptides are abundant in the human brain, their monomer, oligomer, and fibril forms have been studied intensively through experiments[11−14] and molecular simulations.[15,16] Although they differ in just the last two residues, Ile41 and Ala42, they show remarkably distinct behaviors. In a water environment, both the monomers are disordered, but Aβ1-42 has more β-structure than Aβ1-40, in particular, at the C-terminus. Aβ1-42 self-assembles about 1000-fold faster and is far more toxic than Aβ1-40. Using various experimental techniques, including solid-state NMR, it has been established that fibers have a "cross-β" structure, in which Aβ peptides assembled into β-sheets, with β-strands oriented perpendicular to the fibril axis.[1,17] The structures of Aβ oligomers remain largely unknown despite their dominant role in neurotoxicity.

One of the interesting questions that emerges is the role of the last amino acids, Ile41 and Ala42, in making Aβ1-40 and Aβ1-42 peptides behave so differently. It should be noted that several attempts have been made in the past to assess the roles of these two residues in the self-assembly of truncated Aβ peptides. Studying C-terminal fragments of different lengths, it was reported that Ile41 and Ala42 confer a significant increase in the aggregation propensity.[18] Wu et al.[19] probed the structure of 30−40 and 30−42 fragments of Aβ. They found that the longer peptide, Aβ30−42, forms a β-hairpin as a major structural motif. The β-hairpin of Aβ30−42 is converted into a

Received: June 23, 2016
Published: July 8, 2016

DOI: 10.1021/acs.jpcb.6b06368
J. Phys. Chem. B 2016, 120, 7371−7379

turn−coil conformation when the last two hydrophobic residues are removed, suggesting that Ile41 and Ala42 are critical in stabilizing the β-hairpin. However, the roles of these residues in the aggregation propensity of full-length Aβ peptides remain unknown.

To address this question, we have performed in silico and in vitro experiments to compare the structures and aggregation propensities of Aβ1-40, Aβ1-41, and Aβ1-42 peptides. Using replica-exchange molecular dynamics (REMD) and an OPLS-AA/L force field with the generalized Born (GB) implicit solvent, it was shown that the secondary structure contents of the Aβ1-41 monomer are close to those of Aβ1-40 but not to those of Aβ1-42. As the fibril-formation kinetics is governed by intrinsic factors like the secondary structures of monomers, our simulation results suggest that Aβ1-40 and Aβ1-41 have the same order of magnitude of self-assembly rate, which is lower than that for Aβ1-42. This conclusion was further supported by data obtained by the thioflavin-T (Th-T) fluorescence assay. Thus, our in silico and in vitro studies have revealed an important role of the last residue, Ala42, which leads to a huge difference in the aggregation kinetics of Aβ1-40 and Aβ1-42.

2. MATERIALS AND METHODS

2.1. Initial Structures of Aβ Peptides. The structure of the Aβ1-42 peptide used for REMD simulations was taken from the Protein Data Bank,[20] with the code 1Z0Q.[20] The initial structures of Aβ1-41 and Aβ1-40 were obtained from that of Aβ1-42 by removing residues Ala42 and Ile41, respectively. The Aβ1-42 peptide is divided into four regions: the N-terminus (residues 1−16), the central hydrophobic core (residues 17−21), the fibril-loop region (residues 22−29), and the C-terminus (residues 30−42).

2.2. Molecular Dynamics (MD) Simulations. To run MD simulations, we use GROMACS software, version 4.5.5,[21] with the OPLS-AA/L force field.[22] The implicit solvent was implemented by the GB model.[23] The OPLS-AA force field was chosen because it generated conformations for the Aβ1-42 monomer that matched the structure of the Aβ peptide obtained from the NMR data.[15] Additionally, previous studies demonstrated that this force field is suitable for simulation of the aggregation of various Aβ fragments.[1] Moreover, Aβ1-40, Aβ1-41, and Aβ1-42 were simulated under the same conditions for comparison; the choice of force field would not affect our conclusion much.

We choose the GB implicit solvent not only because of limitations in our resources but also because prior studies showed that the GB model gives reasonable results for Aβ variants[16,24] and other systems.[25,26] One of the limitations of the implicit solvent is that it ignores the interactions with water. Therefore, the success of the GB approximation in studying Aβ thermodynamics[16,24] is presumably due to the fact that water bridges do not contribute significantly to the stability of highly flexible molecules, such as intrinsically disordered Aβ.[16]

The leapfrog algorithm[27] was implemented to integrate equations of motion, with a time step of 2 fs. The length of all bonds was constrained by the LINCS algorithm.[28] The velocity-rescaling method proposed by Bussi et al.[29] was used to change the velocity of the atoms periodically, but the temperature of the system was kept stable, with a relaxation time of 0.1 ps. This method is known to be efficient in generating a proper canonical ensemble, which is important for REMD performance.

In implicit solvent models, solvation free energy G_{solv} is the sum of three terms, a solvent−solvent cavity term, G_{cav}; a solute−solvent van der Waals term, G_{vdw}; and, finally, a solvent−solute electrostatics polarization term, G_{pol}. The sum of G_{cav} and G_{vdw} corresponds to the nonpolar free energy of solvation for a molecule from which all charges have been removed, and it is commonly called G_{np}. Then, the total solvation free energy becomes $G_{solv} = G_{np} + G_{pol}$. Here, G_{np} is computed as the total solvent accessible surface area (SASA) multiplied with surface tension,[23] $G_{np} = \gamma \times \mathrm{SASA}$ and $\gamma = 0.005$ kcal/(mol Å^2). G_{pol} is calculated from the analytic GB equation.[30]

We used 12 replicas for REMD simulations for all systems. The temperatures of the replicas were chosen using the method of Patriksson and van der Spoel.[31] The range of temperatures was from 290.16 to 490.16 K for all systems (T = 290.16, 300, 311.80, 326.18, 343.14, 361.92, 380.83, 400.69, 421.86, 444.02, 466.14, and 490.16 K). With this temperature set, the replica acceptance rate was about 20%. An attempt to exchange replicas was made every 2 ps, which is large enough compared to the coupling time to the heat bath. Each replica was run for 1000 ns, and data were collected every 10 ps for data analysis.

2.3. Tools and Measures Used for Data Analysis. *2.3.1. Secondary Structure.* The STRIDE algorithm[32,33] was used to calculate the secondary structures of Aβ peptides. The advantage of this algorithm is that it is based not only on dihedral angles but also on hydrogen bonds.

2.3.2. Salt Bridge (SB). An SB between two oppositely charged residues is considered as having been formed if the distance between two specific atoms remains within 4.6 Å. For Asp23-Lys28 SB, we considered the distance between the C^{γ} atom of Asp23 and N^{ζ} atom of Lys28.

2.3.3. Contact Map. To construct side-chain contact maps, we calculated the distance between the centers of masses of two residues. If this distance is within 6.5 Å, then the corresponding contact is formed.

2.3.4. Free-Energy Landscape. We calculated the free energy of systems as $\Delta G(V) = -k_B T\,[\ln P(V) - \ln P_{max}]$, where $P(V)$ is the probability distribution obtained from the MD simulation for reaction coordinates V. P_{max} is the maximum of the distribution, which corresponds to the lowest-free-energy minimum, $\Delta G = 0$. The two most important eigenvalues, V_1 and V_2, in the dihedral principal component analysis (dPCA)[34] were used as reaction coordinates for constructing the free-energy surface.

2.4. In Vitro Experiment. *2.4.1. Synthesis and Purification of Aβ Peptides.* Aβ1-40, Aβ1-41, and Aβ1-42 were synthesized in an ABI 433A solid-phase peptide synthesizer, using the fluorenylmethyloxycarbonyl protocol, with *p*-hydroxymethylphenoxymethyl polystyrene resin. Cleavage and deprotection of the synthesized peptides were performed by treatment with a mixture of trifluoroacetic acid/distilled water/phenol/thioanisole/ethanedithiol. Then, the peptides were extracted using diethyl ether/H_2O (1:1, v:v) with 0.1% 2-mercaptoethanol. To keep most Aβ peptides in the monomeric state, the synthesized Aβ peptides were dissolved in hexafluoroisopropanol (HFIP), centrifuged at 15 000*g* for 30 min, and the insoluble particles were discarded. The supernatant was then purified on a reverse-phase C-18 high-pressure liquid chromatography column, with a linear gradient from 0 to 80% acetonitrile (with H_2O containing 0.1% NaOH). The pools containing Aβ monomers were collected and dried using a vacuum freeze dryer and stored at −80 °C. The molecular

DOI: 10.1021/acs.jpcb.6b06368
J. Phys. Chem. B 2016, 120, 7371−7379

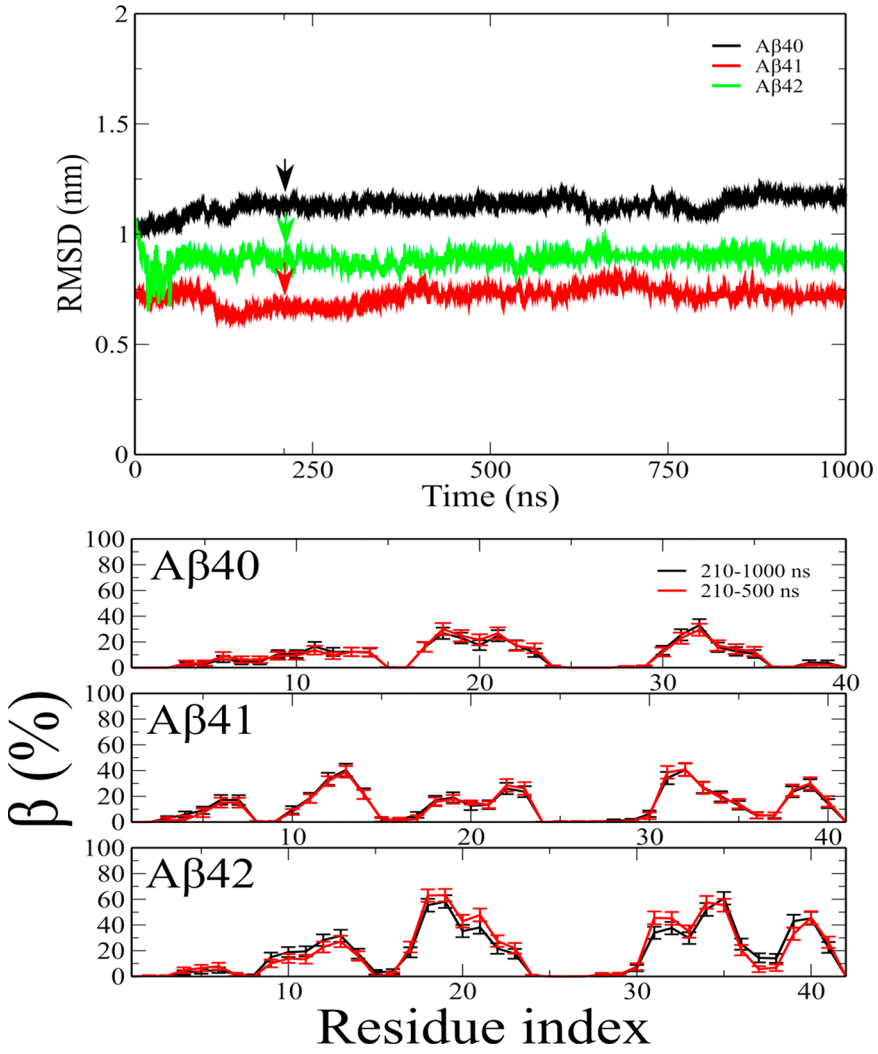

Figure 1. (Upper part) Time dependence of Cα-RMSD at T = 311.8 K for the three sequences. The arrow refers to equilibration time $t_{eq} \approx 210$ ns when the RMSD saturates. (Lower part) The β-content obtained for two time windows at T = 311.8 K for the three peptides. Black and red refer to windows [210−1000 ns] and [210−500 ns], respectively. Error bars are obtained by averaging over snapshots collected at equilibrium.

weights of Aβ peptides were verified by matrix-assisted laser desorption ionization time-of-flight mass spectroscopy.

2.4.2. Aggregation Assay. The aggregation state of Aβ peptides was detected using the Th-T assay.[35] The Aβ peptide stock solution was made by dissolving 2 mg of lyophilized Aβ peptides in 1 mL HFIP/100 mM NaOH (50:50, v/v), and it was stored at −150 °C until use. To examine the aggregation kinetics, a final peptide concentration of 10 μM was diluted from the peptide stock solution in 25 mM phosphate buffer (pH 7.4) with 5 μM Th-T and 0.01% NaN_3. Th-T fluorescence measurements were performed on a microplate reader with a button read mode (FlexStation 3, MD) every 10 min at 37.0 ± 0.2 °C. The excitation and emission wavelengths were 440 and 485 nm, respectively. The kinetic assay was reported as the average sum of three separate analyses (each analysis contained three individual samples for each Aβ peptide).

3. RESULTS

3.1. REMD Simulation. Although the MD simulation has been carried out for 12 temperatures, we will focus on T = 311.8 K, which is closest to the physiological temperature T = 37 °C (310 K).

3.1.1. Equilibration. The REMD runs were performed for total time t_{full} = 1000 ns for all three peptides. To obtain equilibration time t_{eq}, we have monitored the Cα-root-mean-square displacement (RMSD) as a function of time (Figure 1). Defining t_{eq} as the time when RMSD reaches saturation, we obtained $t_{eq} \approx 210$ ns for the three sequences.

To ascertain that our data are well equilibrated we have adopted the following procedure. We perform one MD run with duration t_1 and another that is 2-fold longer than the first run, $t_2 = 2t_1$. If relevant quantities calculated at equilibrium for the two runs coincide, then the system can be considered well equilibrated. Because in our case t_1 = 500 ns, $t_2 = t_{full}$ = 1000 ns, and t_{eq} = 210 ns, secondary structures were computed in two time windows, $[t_{eq}, t_1]$ and $[t_{eq}, t_{full}]$ or [210, 500 ns] and [210, 1000 ns]. Excluding the first 210 ns spent on equilibration, we have obtained the β-content at T = 311.8 K for Aβ1-40, Aβ1-41, and Aβ1-42 (Figure 1). It seems that the error bars obtained for the wider time window should be smaller than those for the narrower window because it is well known that the error bar of a quantity described by entirely random numbers should decay with the number of samples, N, as $N^{-1/2}$. In our case, all quantities are measured at equilibrium, that is, they fluctuate around the mean equilibrium value not being

DOI: 10.1021/acs.jpcb.6b06368
J. Phys. Chem. B 2016, 120, 7371−7379

random variables. Therefore, the error bars should not depend on the number of collected snapshots, as seen in Figure 1. Clearly, within error bars, the two time windows provide the same β-content. This is also valid for helix, turn, and coil structures (results not shown), implying that our replica exchange simulations afford the equilibrated data for all studied systems. In what follows, we will present the results obtained in the $[t_{eq}, t_{full}]$ window.

3.1.2. Secondary Structures of Aβ1-40. Using snapshots collected at equilibrium at 311.8 K for Aβ1-40, we obtained 11.97, 3.89, 65.69, and 18.45% for mean β, helix, turn, and coil structures, respectively (Table 1). Low β (11.97%) and helix (3.89%) percentages are consistent with the experimental results reported by Zhang et al.[36] and Danielsson et al.,[37] showing that the Alzheimer's Aβ peptide adopts a collapsed coil structure in an aqueous environment. Note that using the same OPLS-AA/L force field Truong et al.[24] obtained an α-helix content of 0.2 ± 1.3%, which is lower than the present estimate. This discrepancy arises from the different replica exchange rate and temperature window used by us. On filtration through a filter with a 10 000 molecular-weight cutoff, circular dichroism of low-molecular-weight Aβ1-40 aggregates gives 88% random coil and turn, 12% β-strand, and 0% α-helix structures at pH 7.5 and 295 K on day 0.[38] In contrast, another preparation of Aβ1-40 aggregates gives a 25% β-strand structure for the monomer.[39] Our findings of 84% turn + coil and 12% β structures are perfectly in line with those from the first preparation (88 and 12%).

Table 1. Mean Secondary Structures of Aβ1-40, Aβ1-41, and Aβ1-42 Estimated at Equilibrium, at T = 311.8 K[a]

content (%)	Aβ1-40	Aβ1-41	Aβ1-42
β	11.97 ± 1.44	14.52 ± 1.89	21.95 ± 1.91
α	3.89 ± 1.23	1.93 ± 1.74	2.09 ± 1.70
turn	65.69 ± 9.72	66.45 ± 9.19	60.01 ± 7.72
coil	18.45 ± 3.54	17.10 ± 3.10	15.95 ± 3.23

[a]Error bars come from averaging over snapshots collected at equilibrium. Here, error bar δr of quantity r was computed using the standard formula $\delta r = \sqrt{\frac{1}{N}\sum_{i=1}^{N}(r_i - \langle r\rangle)^2}$, $\langle r\rangle = \frac{1}{N}\sum_{i=1}^{N} r_i$, where N is the number of collected snapshots.

Present simulations show the α-content to be lower than that in the prior coarse-grained UNRES[40] estimation but comparable to the all-atom results of Viet et al.[41,42] and Truong et al.[24] Our estimate of β-content (12%) is also compatible with the results reported by Sgourakis et al.[15] and Yang and Teplow,[16] who have used Amber-derived PARM94, PARM96, MOD-PARM, GROMOS, OPLS, and an improved version of Amber force field PARM99SB to study the dynamics of Aβ peptides in aqueous solution. The REMD simulation protocol coupled with the OPLS-AA/L force field and TIP3P water model yields[43] $\beta \approx 25\%$, which seems to be high and far from the experimental data for Aβ1-40.[37] The discrete MD simulation using the four-bead protein model gives $\beta \approx 19\%$ for full-length Aβ1-40 and 15% for truncated Aβ3−40.[44] These estimations are slightly higher than ours.

3.1.3. Secondary Structures of Aβ1-42. We first compare our results obtained using the OPLS force field coupled with implicit solvent for Aβ1-42 with those from previous studies. The β-content of Aβ1-42 (22%) is markedly higher than that of Aβ1-40 (12%) (Table 1 and Figure 1). This result agrees with that reported in theoretical works[15,16,41,45−47] and the experimental data[48] that Aβ1-42 self-assembles much faster than Aβ1-40 due to the higher population of fibril-prone state N*.[49]

The rich β-propensity appearing at residues 18−21 (Figure 2) is consistent with the findings of Rosenman et al.,[43] who obtained a high β-structure at residues 16−23 using the OPLS-AA/L force field with explicit water model TIP3P. Using the Amber ff99SB force field and TIP4P-Ew water model, one can demonstrate that the 16−21 region is also rich in β-structure.[50] The C-terminus has a high β-structure at residues 31−35 and 39−41 (Figure 2), whereas previous theoretical studies have shown that it is predominantly located in regions 38−41,[15] 32−36,[16] 27−37,[43] 29−36,[50] and 37−40.[42] The C-terminus of Aβ1-

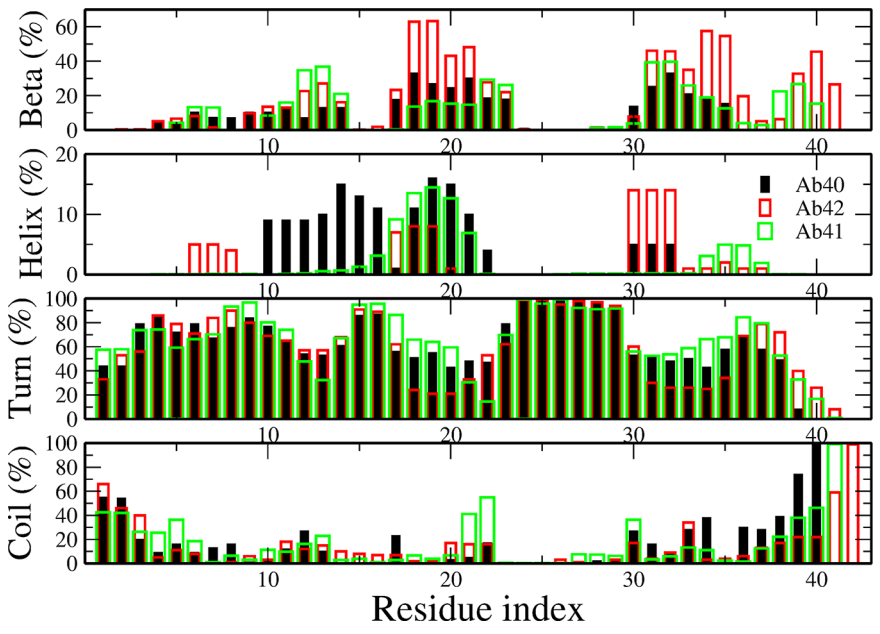

Figure 2. Per-residue distributions of secondary structures of Aβ1-40, Aβ1-41, and Aβ1-42 at 311.8 K. Results were obtained at equilibrium.

DOI: 10.1021/acs.jpcb.6b06368
J. Phys. Chem. B 2016, 120, 7371−7379

42 is much more ordered than the N-terminus, in agreement with the experimental fact that the C-terminus is fibril-prone[14] and with the MD simulations observing the fibril growth to initiate from this end.[51] Contrary to our and other theoretical studies, it was reported that the C-terminus is poorer in β-propensity than the N-terminus,[52] using the coarse-grained model, OPEP. This may be due to approximations adopted in the coarse-graining and implicit solvent approximations. A β-strand was also predicted in the N-terminus using the discrete MD simulation of the four-bead model.[46] Our value of β-content is slightly higher than that of Velez-Vega and Escobedo,[53] Yang and Teplow,[16] and Cote et al.,[52] but it is considerably less than that estimated by Mitternacht et al.[54] The abundance of β-structure reported by the latter authors is presumably due to omission of electrostatic interactions in their models.[55] Similar to that of Aβ1-40, the α-content of Aβ1-42 is nearly zero (Table 1), in agreement with that in other groups,[52,53,56] but it is lower than the prediction of Yang and Teplow.[16] At equilibrium, the random coil structure (coil + turn) is 75.9% (Table 1), implying that Aβ1-42 is more structured than Aβ1-40, which has an 84.1% random coil structure. Our estimations fall into the range of other theoretical results[15,16,52,53] but are lower than those of Mitternacht et al.[54]

3.1.4. Secondary Structures of Aβ1-41. The addition of residues Ile41 to Aβ1-40 increases the β-content from about 12 to 14.5%, which is notably lower than the 22% β-content of Aβ1-42 (Table 1). Thus, the mean β-propensity of Aβ1-41 is much closer to that of Aβ1-40 than to that of Aβ1-42, highlighting the importance of the last residue, Ala42. The high similarity in the β-structures of Aβ1-40 and Aβ1-41 monomers is also visible from per-residue distributions (Figure 2), showing that both peptides have fibril-prone regions, 18−23 and 31−34, populated with β-structure. In the N-terminus, Aβ1-41 has a higher β-propensity at residues 12 and 13 than that in Aβ1-40, but this effect is compensated by the lower β-content at 18 and 21. The C-terminus of Aβ1-41 is more ordered than that of Aβ1-40, having a more β-structure at residues 38 and 39. The rigidity of the C-terminus of Aβ1-42 is obviously higher than that of Aβ1-40 and Aβ1-41 (Figure 2). Because the flexibility of this end controls the self-assembly rate, one can expect that Aβ1-42 aggregates faster than not only Aβ1-40 but also Aβ1-41. Such an expectation is further supported by the domination of β-content in the fibril-prone region, 18−21, at the N-terminus in Aβ1-42.

In an experimental study,[57] Teplow and his collaborators demonstrated that Aβ1-40 and Aβ1-42 oligomerize through distinct pathways. Although both Ile41 and Ala42 accelerate aggregation, Ile41 is critical for the formation of small oligomers composed of four to five monomers (paranuclei), which are absent in Aβ1-40. Ala42, on the other hand, promotes the formation of larger oligomers composed of several paranuclei. Thus, the fact that Ala42 facilitates β-sheet formation to a greater extent than that by Ile41 seems to be consistent with these results.

There is a minor difference in the mean values of the helix and coil contents of the three variants (Table 1). Per-residue helix distributions are distinct for the three variants, but this would not have had a big impact on the difference in their behaviors because the helix level itself is low. Distinctions in the coil contents of the three peptides are observed at a few residues, including 21, 22, and 41, at which the coil propensity of Aβ1-41 is higher than that of Aβ1-40 and Aβ1-42 (Figure 2). The coil substantially levels up at residues 39 and 42 for Aβ1-40 and 1, 42, and 42 for Aβ1-42, which may affect the aggregation kinetics of these peptides. The distributions of turns of the three variants are rather similar, particularly in the turn region 22−29, suggesting that the last residues, Ile41 and Ala42, have minor impacts on turn propensity.

3.1.5. SB Asp23−Lys28. Because SB Asp23−Lys28 plays a crucial role in the formation of cross-β structures of fibrils,[58] we study it in detail. The distributions of distances between atoms C_{23}^{γ} and N_{28}^{ζ} of Aβ1-40 and Aβ1-41 are similar, having two peaks (Figure 3). The corresponding distribution of Aβ1-42 has a high peak located at a relatively short distance, implying that SB Asp23-Lys28 of this peptide is less flexible compared to that of Aβ1-40 and Aβ1-41. This result is also supported by our data, showing that the mean SB distance of Aβ1-42 (7.97 Å) is shorter than that of Aβ1-40 (8.59 Å) and Aβ1-41 (8.69 Å). The reduced flexibility due to Ala42 is in agreement with the experimental observation that Aβ1-42 self-assembles faster than Aβ1-40. As shown below by the Th-T fluorescence assay, this conclusion also holds, comparing Aβ1-42 aggregation kinetics with that of Aβ1-41.

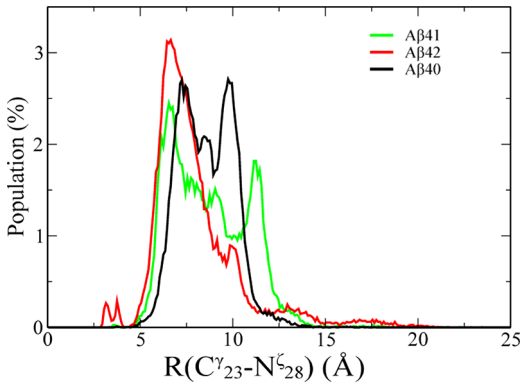

Figure 3. Distributions of SB Asp23−Lys28 distances of $A\beta_{40}$, $A\beta_{41}$, and $A\beta_{42}$ at 311.8 K. The mean distances are 7.97, 8.69, and 8.59 Å for Aβ1-42, Aβ1-41, and Aβ1-40, respectively.

3.1.6. SB Contact Map. Figure 4 shows the contact maps of all 18 SBs formed by three positively and six negatively charged residues for the three variants. Clearly, the maps of Aβ1-40 and Aβ1-41 are nearly the same, except that the Arg5-Glu22 population of Aβ40 (21%) is higher than that of Aβ1-41 (0.2%). The addition of Ala42 substantially promotes the formation of SB Arg5−Glu11 in Aβ1-42 (25%) compared to that in Aβ1-40 (2%) and Aβ1-41 (2%). The same also holds for the formation of SB Arg5−Glu22 in Aβ1-42 (41.2%), which is remarkably higher than that in Aβ1-40 and Aβ1-41. The population of SB Asp23−Lys28 is about 51, 50, and 68% in Aβ1-40, Aβ1-41, and Aβ1-42, respectively. Thus, the impact of residue Ala42 is not only on the enhanced rigidity of this important SB but also on the entire SB network, making Aβ1-42 remarkably distinct from the shorter variants.

3.1.7. Free Energy Surfaces. Using V_1 and V_2 from the dPCA analysis as reaction coordinates, free-energy surfaces were constructed for the three peptides at T = 311.8 K (Figure 5). For Aβ1-40, the β-content is populated in representative structures S5 (30%) and S6 (20%) (see also Table 2), which are compatible with the most dominant structures reported in previous studies by Rosenman et al.[43] and Ball et al.[50] The α-content is relatively high (15%) for S3, but it is zero for the

DOI: 10.1021/acs.jpcb.6b06368
J. Phys. Chem. B 2016, 120, 7371−7379

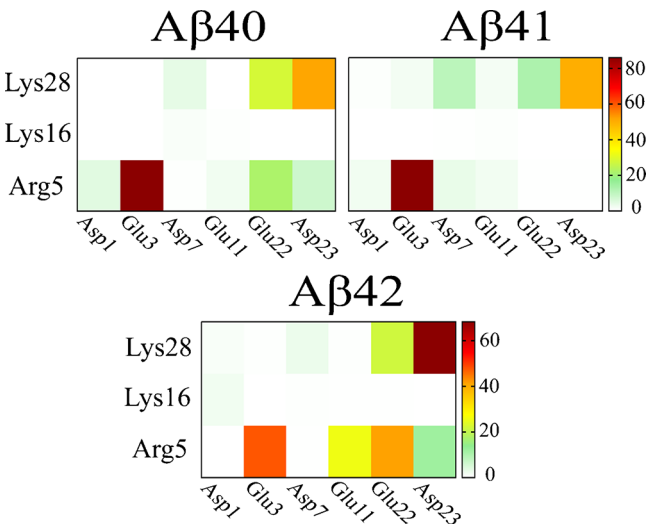

Figure 4. SB contact maps obtained at equilibrium at T = 311.8 K using the definition of side-chain contact described in Section 2.

others. The turn varies between 45 and 71%, whereas the coil changes from 15% (S3) to 41% (S2).

In Aβ1-41, three basins, 1, 4, and 6, are populated by β-structures, resulting in a slight increase in β compared to that in Aβ1-40. This effect is observed upon addition of hydrophobic residue Ile41. Contrary to that in Aβ1-40, none of the representative structures possess a helical structure (Table 2 and Figure 6). Overall, the turn of S1−S6 is slightly higher than that in Aβ1-40, falling in the region between 51 and 78%. In return, the coil is slightly lower (5−29%).

Table 2. Characterizations of Structures (S) Representing Major Basins on the Free Energy Surface of Aβ1-40, Aβ1-41, and Aβ1-42 in Figure 5[a]

system	S	P (%)	β	α	turn	coil
Aβ1-40	1	22.7	0.0	0.0	65.0	35.0
	2	17.9	0.0	0.0	58.8	41.2
	3	16.4	0.0	15.0	70.0	15.0
	4	14.2	0.0	0.0	77.5	22.5
	5	12.6	30.0	0.0	45.0	25.0
	6	11.6	20.0	0.0	55.0	25.0
Aβ1-41	1	20.5	19.5	0.0	75.6	4.9
	2	16.5	0.0	0.0	75.6	24.4
	3	14.9	0.0	0.0	78.0	22.0
	4	14.1	22.0	0.0	51.2	26.8
	5	13.7	0.0	0.0	70.7	29.3
	6	12.1	12.2	0.0	51.2	26.8
Aβ1-42	1	19.0	14.3	0.0	73.8	11.9
	2	18.5	19.0	7.1	59.5	14.4
	3	17.1	23.8	0.0	57.2	19.0
	4	14.8	23.8	0.0	54.8	21.4
	5	11.6	0.0	0.0	75.0	25.0
	6	9.7	23.8	0.0	71.4	4.8

[a]The third column refers to the population of basins.

In contrast to that in Aβ1-40 and Aβ1-41, except S5 the dominant structures of Aβ1-42 are populated with the β-structure, confirming that the addition of Ala42 makes the monomer structure more ordered. As the monomer can serve as a precursor for the formation of fibrils with cross-β structures, the increased β-content facilitates amyloid self-assembly.[1,49] Only S2 contains a short helix (7%). Similar to that in Aβ1-41, the coil and turn of representative structures of

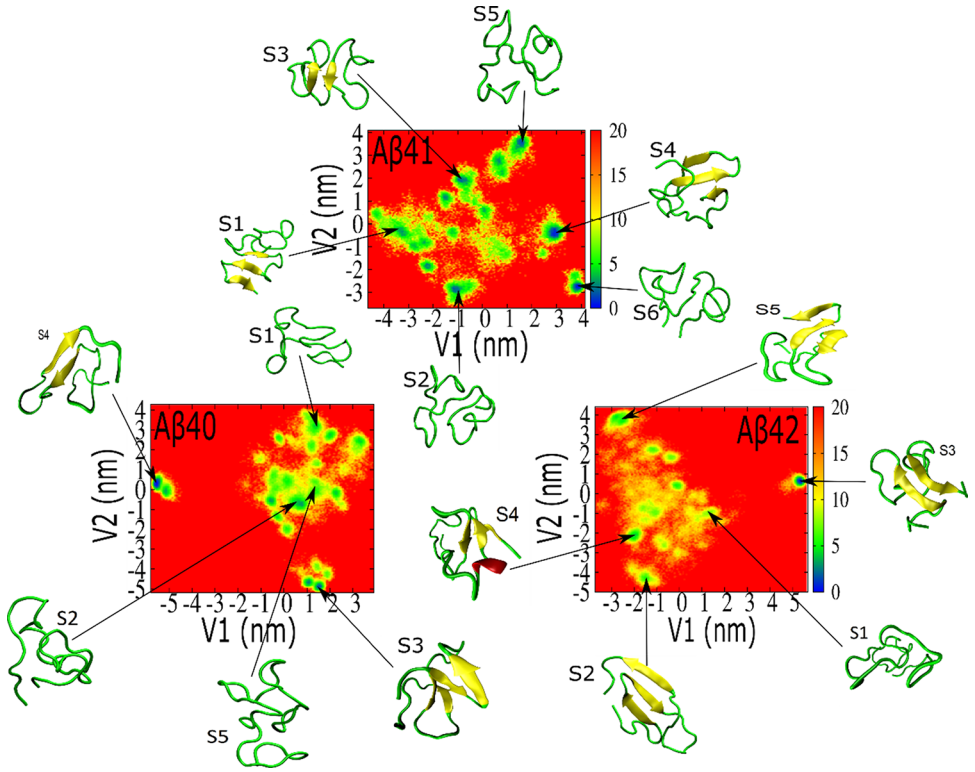

Figure 5. Free-energy surfaces of Aβ_{40}, Aβ_{41}, and Aβ_{42} as a function of the first two principal components, $V1$ and $V2$. Results were obtained at equilibrium and T = 311.8 K. Shown are representative snapshots obtained by the clustering method.

DOI: 10.1021/acs.jpcb.6b06368
J. Phys. Chem. B 2016, 120, 7371−7379

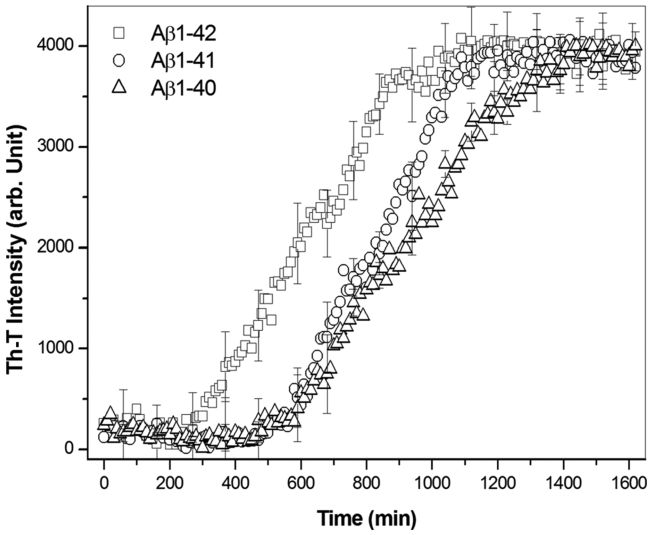

Figure 6. Aggregation kinetics of Aβ1-42 (□), Aβ1-41 (○), and Aβ1-40 (△), determined by the Th-T fluorescence assay. (Means and SDs are plotted, n = 9.)

Aβ1-42 fall in the range of 5−25 and 55−75%, respectively. Overall, local minima of Aβ1-42 are shallower than those of Aβ1-40 and Aβ1-41, consistent with the fact that Aβ1-42 is more fibril-prone.

3.2. Aggregation Kinetics. Figure 6 shows the aggregation process for Aβ1-42, Aβ1-41, and Aβ1-40, detected by the Th-T fluorescence assay at T = 37 °C. Obviously, all curves are sigmoidal in shape indicating that the aggregation kinetics of Aβ1-42, Aβ1-41, and Aβ1-40 is a three-stage process involving nucleation, elongation, and fibrillation. The Th-T intensity for Aβ1-42 reached the steady state in 15 h, whereas for both Aβ1-41 and Aβ1-40, the steady state of Th-T fluorescence intensity was reached in around 18−20 h. The lag phase for Aβ1-41 and Aβ1-40 was similar, whereas the lag phase for Aβ1-42 was obviously shorter than that for Aβ1-41 and Aβ1-40. The duration of the lag phase for Aβ1-42, Aβ1-41, and Aβ1-40 was around 3, 8, and 8.5, respectively.

By fitting the kinetic curve with a simple Boltzmann sigmoidal function, the obtained $t_{1/2}$ values were 604.4 ± 2.0, 831.1 ± 3.4, and 937.1 ± 5.2 min for Aβ1-42, Aβ1-41, and Aβ1-40, respectively. The difference in the aggregation rate between Aβ1-40 and Aβ1-41 is less than that between Aβ1-41 and Aβ1-42. Taken together, our results indicate that the aggregation rate for Aβ1-42 is faster than that for Aβ1-40 and Aβ1-41. Our in vitro results suggest that residue Ala42, rather than Ile41, may play a more important role in Aβ aggregation. This is consistent with the findings of our simulation study.

4. CONCLUSIONS

Using the all-atom REMD simulation with implicit water, we have shown that the secondary structures of Aβ1-40 and Aβ1-41 and their per-residue distributions are similar, but they are different from those of Aβ1-42. Thus, residue Ile41 does not modulate the monomer structures and, consequently, the self-assembly propensity of Aβ much. The addition of hydrophobic residue Ala42 radically changes the structure and dynamics of monomers, leveling up the β-content and rigidity of SB Asp23-Lys28. The enhanced β-content population in fibril-prone regions in the monomer state is expected to speed up aggregation of Aβ1-42 to a much larger extent compared to that in Aβ1-41. Because monitoring fibril formation of full-length Aβ peptides by computer simulation is beyond the present computational facilities, we performed Th-T fluorescence measurements, which showed that Aβ1-40 and Aβ1-41 indeed aggregate much slower than Aβ1-42 and their self-assembly rates have the same orders of magnitude. Taken together, both in silico and in vitro experiments have ascertained the importance of Ala42 in the structure and aggregation kinetics of Aβ. It would be interesting to know to what extent the interchange of Ile41 and Ala42 in a sequence alters the aggregation properties.

AUTHOR INFORMATION

Corresponding Authors

*E-mail: chen15@mmc.edu.tw. Tel: +886-2-26363030 #1234 (Y.-C.C.).

*E-mail: masli@ifpan.edu.pl. Tel: +48 22 843 66 01 (M.S.L.).

Author Contributions

M.S.L. and Y.-C.C. conceived the experiments. N.H.L., M.H.V., P.M.T., and T.M.T. conducted the experiment. N.H.L., M.H.V., P.M.T., P.D.L., T.M.T., P.H.N., M.S.L., and Y.-C.C. analyzed the results. N.H.L., T.M.T., M.S.L., and Y.-C.C. wrote the paper. All authors reviewed the manuscript.

Notes

The authors declare no competing financial interest.

ACKNOWLEDGMENTS

This work was supported by the Department of Science and Technology at Ho Chi Minh city, Vietnam, the Polish NCN grant 2015/19/B/ST4/02721, grants from the Ministry of Science and Technology, ROC (MOST104-488 2627-M-715-001 to Y.-C.C.), and Mackay Medical College (102B05 and 103B06 to Y.-C.C.). We thank E.P. O'Brien for critical reading of the manuscript.

REFERENCES

(1) Nasica-Labouze, J.; Nguyen, P. H.; Sterpone, F.; Berthoumieu, O.; Buchete, N. V.; Cote, S.; De Simone, A.; Doig, A. J.; Faller, P.; Garcia, A.; et al. Amyloid Beta Protein and Alzheimer's Disease: When Computer Simulations Complement Experimental Studies. *Chem. Rev.* **2015**, *115*, 3518−3563.

(2) Um, J. W.; Kaufman, A. C.; Kostylev, M.; Heiss, J. K.; Stagi, M.; Takahashi, H.; Kerrisk, M. E.; Vortmeyer, A.; Wisniewski, T.; Koleske, A. J.; et al. Metabotropic Glutamate Receptor 5 Is a Coreceptor for Alzheimer A Beta Oligomer Bound to Cellular Prion Protein. *Neuron* **2013**, *79*, 887−902.

(3) Rembach, A.; Faux, N. G.; Watt, A. D.; Pertile, K. K.; Rumble, R. L.; Trounson, B. O.; Fowler, C. J.; Roberts, B. R.; Perez, K. A.; Li, Q. X.; et al. Changes in Plasma Amyloid Beta in a Longitudinal Study of Aging and Alzheimer's Disease. *Alzheimer's Dementia* **2014**, *10*, 53−61.

(4) Qi-Takahara, Y.; Morishima-Kawashima, M.; Tanimura, Y.; Dolios, G.; Hirotani, N.; Horikoshi, Y.; Kametani, F.; Maeda, M.; Saido, T. C.; Wang, R.; et al. Longer Forms of Amyloid Beta Protein: Implications for the Mechanism of Intramembrane Cleavage by Gamma-Secretase. *J. Neurosci.* **2005**, *25*, 436−445.

(5) Yagishita, S.; Morishima-Kawashima, M.; Tanimura, Y.; Ishiura, S.; Ihara, Y. Dapt-Induced Intracellular Accumulations of Longer Amyloid Beta-Proteins: Further Implications for the Mechanism of Intramembrane Cleavage by Gamma-Secretase. *Biochemistry* **2006**, *45*, 3952−3960.

(6) Van Vickle, G. D.; Esh, C. L.; Kalback, W. M.; Patton, R. L.; Luehrs, D. C.; Kokjohn, T. A.; Fifield, F. G.; Fraser, P. E.; Westaway, D.; McLaurin, J.; et al. Tgcrnd8 Amyloid Precursor Protein Transgenic Mice Exhibit an Altered Gamma-Secretase Processing and an

DOI: 10.1021/acs.jpcb.6b06368
J. Phys. Chem. B 2016, 120, 7371−7379

Aggressive, Additive Amyloid Pathology Subject to Immunotherapeutic Modulation. *Biochemistry* **2007**, *46*, 10317−10327.
(7) Van Vickle, G. D.; Esh, C. L.; Kokjohn, T. A.; Patton, R. L.; Kalback, W. M.; Luehrs, D. C.; Beach, T. G.; Newel, A. J.; Lopera, F.; Ghetti, B.; et al. Presenilin-1 280glu -> Ala Mutation Alters C-Terminal App Processing Yielding Longer A Beta Peptides: Implications for Alzheimer's Disease. *Mol. Med.* **2008**, *14*, 184−194.
(8) Miravalle, L.; Calero, M.; Takao, M.; Roher, A. E.; Ghetti, B.; Vidal, R. Amino-Terminally Truncated A Beta Peptide Species are the Main Component of Cotton Wool Plaques. *Biochemistry* **2005**, *44*, 10810−10821.
(9) Sandebring, A.; Welander, H.; Winblad, B.; Graff, C.; Tjernberg, L. O. The Pathogenic A Beta 43 is Enriched in Familial and Sporadic Alzheimer Disease. *PLoS One* **2013**, *8*, e55847.
(10) Burnouf, S.; Gorsky, M. K.; Dols, J.; Gronke, S.; Partridge, L. A Beta(43) Is Neurotoxic and Primes Aggregation of A Beta(40) in Vivo. *Acta Neuropathol.* **2015**, *130*, 35−47.
(11) Petkova, A. T.; Ishii, Y.; Balbach, J. J.; Antzutkin, O. N.; Leapman, R. D.; Delaglio, F.; Tycko, R. A Structural Model for Alzheimer's Beta-Amyloid Fibrils Based on Experimental Constraints from Solid State NMR. *Proc. Natl. Acad. Sci. U.S.A.* **2002**, *99*, 16742−16747.
(12) Petkova, A. T.; Yau, W. M.; Tycko, R. Experimental Constraints on Quaternary Structure in Alzheimer's Beta-Amyloid Fibrils. *Biochemistry* **2006**, *45*, 498−512.
(13) Paravastu, A. K.; Leapman, R. D.; Yau, W. M.; Tycko, R. Molecular Structural Basis for Polymorphism in Alzheimer's Beta-Amyloid Fibrils. *Proc. Natl. Acad. Sci. U.S.A.* **2008**, *105*, 18349−18354.
(14) Luhrs, T.; Ritter, C.; Adrian, M.; Riek-Loher, D.; Bohrmann, B.; Dobeli, H.; Schubert, D.; Riek, R. 3d Structure of Alzheimer's Amyloid-Beta(1−42) Fibrils. *Proc. Natl. Acad. Sci. U.S.A.* **2005**, *102*, 17342−17347.
(15) Sgourakis, N. G.; Yan, Y. L.; McCallum, S. A.; Wang, C. Y.; Garcia, A. E. The Alzheimer's Peptides A Beta 40 and 42 Adopt Distinct Conformations in Water: A Combined MD/NMR Study. *J. Mol. Biol.* **2007**, *368*, 1448−1457.
(16) Yang, M.; Teplow, D. B. Amyloid Beta-Protein Monomer Folding: Free Energy Surfaces Reveal Alloform-Specific Differences. *J. Mol. Biol.* **2008**, *384*, 450−464.
(17) Chiti, F.; Dobson, C. M. Protein Misfolding, Functional Amyloid, and Human Disease. *Annu. Rev. Biochem.* **2006**, *75*, 333−366.
(18) Li, H. Y.; Monien, B. H.; Fradinger, E. A.; Urbanc, B.; Bitan, G. Biophysical Characterization of A Beta 42 C-Terminal Fragments: Inhibitors of A Beta 42 Neurotoxicity. *Biochemistry* **2010**, *49*, 1259−1267.
(19) Wu, C.; Murray, M. M.; Bernstein, S. L.; Condron, M. M.; Bitan, G.; Shea, J. E.; Bowers, M. T. The Structure of A Beta 42 C-Terminal Fragments Probed by a Combined Experimental and Theoretical Study. *J. Mol. Biol.* **2009**, *387*, 492−501.
(20) Tomaselli, S.; Esposito, V.; Vangone, P.; van Nuland, N. A.; Bonvin, A. M.; Guerrini, R.; Tancredi, T.; Temussi, P. A.; Picone, D. The Alpha-to-Beta Conformational Transition of Alzheimer's A Beta-(1−42) Peptide in Aqueous Media is Reversible: A Step by Step Conformational Analysis Suggests the Location of Beta Conformation Seeding. *ChemBiochem* **2006**, *7*, 257−267.
(21) Hess, B.; Kutzner, C.; van der Spoel, D.; Lindahl, E. Gromacs 4: Algorithms for Highly Efficient, Load-Balanced, and Scalable Molecular Simulation. *J. Chem. Theory Comput.* **2008**, *4*, 435−447.
(22) Kaminski, G. A.; Friesner, R. A.; Tirado-Rives, J.; Jorgensen, W. L. Evaluation and Reparametrization of the OPLS-AA Force Field for Proteins Via Comparison with Accurate Quantum Chemical Calculations on Peptides. *J. Phys. Chem. B* **2001**, *105*, 6474−6487.
(23) Onufriev, A.; Bashford, D.; Case, D. A. Exploring Protein Native States and Large-Scale Conformational Changes with a Modified Generalized Born Model. *Proteins: Struct., Funct., Bioinf.* **2004**, *55*, 383−394.
(24) Truong, P. M.; Viet, M. H.; Nguyen, P. H.; Hu, C. K.; Li, M. S. Effect of Taiwan Mutation (D7h) on Structures of Amyloid-Beta Peptides: Replica Exchange Molecular Dynamics Study. *J. Phys. Chem. B* **2014**, *118*, 8972−8981.
(25) Yang, M.; Yordanov, B.; Levy, Y.; Bruschweiler, R.; Huo, S. The Sequence-Dependent Unfolding Pathway Plays a Critical Role in the Amyloidogenicity of Transthyretin. *Biochemistry* **2006**, *45*, 11992−12002.
(26) Lei, H. X.; Wu, C.; Liu, H. G.; Duan, Y. Folding Free-Energy Landscape of Villin Headpiece Subdomain from Molecular Dynamics Simulations. *Proc. Natl. Acad. Sci. U.S.A.* **2007**, *104*, 4925−4930.
(27) Hockney, R. W.; Goel, S. P.; Eastwood, J. Quit High Resolution Computer Models of Plasma. *J. Comput. Phys.* **1974**, *14*, 148−158.
(28) Hess, B.; Bekker, H.; Berendsen, H. J. C.; Fraaije, J. G. E. M. LINCS: A Linear Constraint Solver for Molecular Simulations. *J. Comput. Chem.* **1997**, *18*, 1463−1472.
(29) Bussi, G.; Donadio, D.; Parrinello, M. Canonical Sampling through Velocity Rescaling. *J. Chem. Phys.* **2007**, *126*, No. 014101.
(30) Qiu, D.; Shenkin, P. S.; Hollinger, F. P.; Still, W. C. The Gb/Sa Continuum Model for Solvation. A Fast Analytical Method for the Calculation of Approximate Born Radii. *J. Phys. Chem. A* **1997**, *101*, 3005−3014.
(31) Patriksson, A.; van der Spoel, D. A Temperature Predictor for Parallel Tempering Simulations. *Phys. Chem. Chem. Phys.* **2008**, *10*, 2073−2077.
(32) Frishman, D.; Argos, P. Knowledge-Based Protein Secondary Structure Assignment. *Proteins: Struct., Funct., Bioinf.* **1995**, *23*, 566−579.
(33) Heinig, M.; Frishman, D. Stride: A Web Server for Secondary Structure Assignment from Known Atomic Coordinates of Proteins. *Nucleic Acids Res.* **2004**, *32*, W500−W502.
(34) Mu, Y. G.; Nguyen, P. H.; Stock, G. Energy Landscape of a Small Peptide Revealed by Dihedral Angle Principal Component Analysis. *Proteins: Struct., Funct., Bioinf.* **2005**, *58*, 45−52.
(35) Levine, H. Thioflavine-T Interaction with Synthetic Alzheimer's Disease Beta Amyloid Peptides— Detection of Amyloid Aggregation in Solution. *Protein Sci.* **1993**, *2*, 404−410.
(36) Zhang, S.; Iwata, K.; Lachenmann, M. J.; Peng, J. W.; Li, S.; Stimson, E. R.; Lu, Y.; Felix, A. M.; Maggio, J. E.; Lee, J. P. The Alzheimer's Peptide A Beta Adopts a Collapsed Coil Structure in Water. *J. Struct. Biol.* **2000**, *130*, 130−141.
(37) Danielsson, J.; Jarvet, J.; Damberg, P.; Graslund, A. The Alzheimer Beta-Peptide Shows Temperature-Dependent Transitions between Left-Handed 3(1)-Helix, Beta-Strand and Random Coil Secondary Structures. *FEBS J.* **2005**, *272*, 3938−3949.
(38) Kirkitadze, M. D.; Condron, M. M.; Teplow, D. B. Identification and Characterization of Key Kinetic Intermediates in Amyloid Beta-Protein Fibrillogenesis. *J. Mol. Biol.* **2001**, *312*, 1103−1119.
(39) Ono, K.; Condron, M. M.; Teplow, D. B. Structure-Neurotoxicity Relationships of Amyloid Beta-Protein Oligomers. *Proc. Natl. Acad. Sci. U.S.A.* **2009**, *106*, 14745−14750.
(40) Rojas, A.; Liwo, A.; Browne, D.; Scheraga, H. A. Mechanism of Fiber Assembly: Treatment of A Beta Peptide Aggregation with a Coarse-Grained United-Residue Force Field. *J. Mol. Biol.* **2010**, *404*, 537−552.
(41) Viet, M. H.; Nguyen, P. H.; Ngo, S. T.; Li, M. S.; Derreumaux, P. Effect of the Tottori Familial Disease Mutation (D7n) on the Monomers and Dimers of A Beta40 and A Beta42. *ACS Chem. Neurosci.* **2013**, *4*, 1446−1457.
(42) Viet, M. H.; Li, M. S. Amyloid Peptide A Beta(40) Inhibits Aggregation of A Beta(42): Evidence from Molecular Dynamics Simulations. *J. Chem. Phys.* **2012**, *136*, No. 245105.
(43) Rosenman, D. J.; Connors, C. R.; Chen, W.; Wang, C. Y.; Garcia, A. E. A Beta Monomers Transiently Sample Oligomer and Fibril-Like Configurations: Ensemble Characterization Using a Combined MD/NMR Approach. *J. Mol. Biol.* **2013**, *425*, 3338−3359.
(44) Meral, D.; Urbanc, B. Discrete Molecular Dynamics Study of Oligomer Formation by N-Terminally Truncated Amyloid Beta-Protein. *J. Mol. Biol.* **2013**, *425*, 2260−2275.
(45) Lin, Y. S.; Pande, V. S. Effects of Familial Mutations on the Monomer Structure of A Beta(42). *Biophys. J.* **2012**, *103*, L47−L49.

DOI: 10.1021/acs.jpcb.6b06368
J. Phys. Chem. B 2016, 120, 7371−7379

(46) Lam, A. R.; Teplow, D. B.; Stanley, H. E.; Urbanc, B. Effects of the Arctic (E-22 -> G) Mutation on Amyloid Beta-Protein Folding: Discrete Molecular Dynamics Study. *J. Am. Chem. Soc.* **2008**, *130*, 17413−17422.
(47) Viet, M. H.; Ngo, S. T.; Lam, N. S.; Li, M. S. Inhibition of Aggregation of Amyloid Peptides by Beta-Sheet Breaker Peptides and Their Binding Affinity. *J. Phys. Chem. B* **2011**, *115*, 7433−7446.
(48) Snyder, S. W.; Ladror, U. S.; Wade, W. S.; Wang, G. T.; Barrett, L. W.; Matayoshi, E. D.; Huffaker, H. J.; Krafft, G. A.; Holzman, T. F. Amyloid-Beta Aggregation—Selective Inhibition of Aggregation in Mixtures of Amyloid with Different Lengths. *Biophys. J.* **1994**, *67*, 1216−1228.
(49) Li, M. S.; Co, N. T.; Hu, C. K.; Straub, J. E.; Thirumalai, D. Determination of Factors Governing Fibrillogenesis of Polypeptide Chains Using Lattice Models. *Phys. Rev. Lett.* **2010**, *105*, No. 218101.
(50) Ball, K. A.; Phillips, A. H.; Wemmer, D. E.; Head-Gordon, T. Differences in Beta-Strand Populations of Monomeric A Beta 40 and A Beta 42. *Biophys. J.* **2013**, *104*, 2714−2724.
(51) Han, M.; Hansmann, U. H. E. Replica Exchange Molecular Dynamics of the Thermodynamics of Fibril Growth of Alzheimer's A Beta(42) Peptide. *J. Chem. Phys.* **2011**, *135*, No. 065101.
(52) Cote, S.; Derreumaux, P.; Mousseau, N. Distinct Morphologies for Amyloid Beta Protein Monomer: A Beta(1−40), A Beta(1−42), and A Beta(1−40)(D23n). *J. Chem. Theory Comput.* **2011**, *7*, 2584−2592.
(53) Velez-Vega, C.; Escobedo, F. A. Characterizing the Structural Behavior of Selected A Beta-42 Monomers with Different Solubilities. *J. Phys. Chem. B* **2011**, *115*, 4900−4910.
(54) Mitternacht, S.; Staneva, I.; Hard, T.; Irback, A. Comparing the Folding Free-Energy Landscapes of A Beta 42 Variants with Different Aggregation Properties. *Proteins: Struct., Funct., Bioinf.* **2010**, *78*, 2600−2608.
(55) Irback, A.; Mohanty, S. Folding Thermodynamics of Peptides. *Biophys. J.* **2005**, *88*, 1560−1569.
(56) Sgourakis, N. G.; Merced-Serrano, M.; Boutsidis, C.; Drineas, P.; Du, Z. M.; Wang, C. Y.; Garcia, A. E. Atomic-Level Characterization of the Ensemble of the A Beta(1−42) Monomer in Water Using Unbiased Molecular Dynamics Simulations and Spectral Algorithms. *J. Mol. Biol.* **2011**, *405*, 570−583.
(57) Bitan, G.; Kirkitadze, M. D.; Lomakin, A.; Vollers, S. S.; Benedek, G. B.; Teplow, D. B. Amyloid Beta-Protein (A Beta) Assembly: A Beta 40 and A Beta 42 Oligomerize through Distinct Pathways. *Proc. Natl. Acad. Sci. U.S.A.* **2003**, *100*, 330−335.
(58) Teplow, D. B.; Lazo, N. D.; Bitan, G.; Bernstein, S.; Wyttenbach, T.; Bowers, M. T.; Baumketner, A.; Shea, J. E.; Urbanc, B.; Cruz, L.; et al. Elucidating Amyloid Beta-Protein Folding and Assembly: A Multidisciplinary Approach. *Acc. Chem. Res.* **2006**, *39*, 635−645.

DOI: 10.1021/acs.jpcb.6b06368
J. Phys. Chem. B 2016, 120, 7371−7379